



HAL
open science

Monofunctional pyrenes at carbon nanotube electrodes for direct electron transfer H₂O₂ reduction with HRP and HRP-bacterial nanocellulose

Sara Bocanegra-Rodríguez, Carmen Molins-Legua, Pilar Campíns-Falcó, Fabien Giroud, Andrew Gross, Serge Cosnier

► To cite this version:

Sara Bocanegra-Rodríguez, Carmen Molins-Legua, Pilar Campíns-Falcó, Fabien Giroud, Andrew Gross, et al.. Monofunctional pyrenes at carbon nanotube electrodes for direct electron transfer H₂O₂ reduction with HRP and HRP-bacterial nanocellulose. *Biosensors and Bioelectronics*, 2021, 187, pp.113304. 10.1016/j.bios.2021.113304 . hal-03376324

HAL Id: hal-03376324

<https://hal.science/hal-03376324>

Submitted on 13 Oct 2021

HAL is a multi-disciplinary open access archive for the deposit and dissemination of scientific research documents, whether they are published or not. The documents may come from teaching and research institutions in France or abroad, or from public or private research centers.

L'archive ouverte pluridisciplinaire **HAL**, est destinée au dépôt et à la diffusion de documents scientifiques de niveau recherche, publiés ou non, émanant des établissements d'enseignement et de recherche français ou étrangers, des laboratoires publics ou privés.

Monofunctional pyrenes at carbon nanotube electrodes for direct electron transfer H₂O₂ reduction with HRP and HRP-bacterial nanocellulose

Sara Bocanegra Rodríguez^[a], Carmen Molins-Legua^[a], Pilar Campíns-Falcó^[a], Fabien Giroud^[b], Andrew J. Gross^{[b]*} and Serge Cosnier^{[b]*}

[a] S. Bocanegra Rodríguez, Carmens Molins-Legua, Pilar Campíns-Falcó
Departament de Química Analítica,
Facultat de Química
Universitat de València,
Dr. Moliner 50, 46100 Burjassot, Valencia (Spain)

[b] F. Giroud, A. Gross, S. Cosnier
Département de Chimie Moléculaire (DCM)
Univ. Grenoble Alpes - CNRS
570 rue de la Chimie, 38041 Grenoble (France)
Email : andrew.gross@univ-grenoble-alpes.fr; serge.cosnier@univ-grenoble-alpes.fr

Abstract

The non-covalent modification of carbon nanotube electrodes with pyrene derivatives is a versatile approach to enhance the electrical wiring of enzymes for biosensors and biofuel cells. We report here a comparative study of five pyrene derivatives adsorbed at multi-walled carbon nanotube electrodes to shed light on their ability to promote direct electron transfer with horseradish peroxidase (HRP) for H₂O₂ reduction. In all cases, pyrene-modified electrodes enhanced catalytic reduction compared to the unmodified electrodes. The pyrene N-hydroxysuccinimide (NHS) ester derivative provided access to the highest catalytic current of 1.4 mA cm⁻² at 6 mmol L⁻¹ H₂O₂, high onset potential of 0.61 V vs. Ag/AgCl, insensitivity to parasitic H₂O₂ oxidation, and a large linear dynamic range that benefits from insensitivity to HRP “suicide inactivation” at 4 to 6 mmol L⁻¹ H₂O₂. Pyrene-aliphatic carboxylic acid groups offer better sensor sensitivity and higher catalytic currents at ≤ 1 mmol L⁻¹ H₂O₂ concentrations. The butyric acid and NHS ester derivatives gave high analytical sensitivities of 5.63 A M⁻¹ cm⁻² and 2.96 A M⁻¹ cm⁻², respectively, over a wide range (0.25 to 4 mmol L⁻¹) compared to existing carbon-based HRP biosensor electrodes. A bacterial nanocellulose pyrene-NHS HRP bioelectrode was subsequently elaborated via “one-pot” and “layer-by-layer” strategies. The optimised bioelectrode exhibited slightly weaker voltage output, further enhanced catalytic currents, and a major enhancement in 1-week stability with 67% activity remaining compared to 39% at the equivalent electrode without nanocellulose, thus offering excellent prospects for biosensing and biofuel cell applications.

Keywords: Direct electron transfer • horseradish peroxidase • biofuel cell cathode • nanocellulose electrode • bioelectrocatalysis • electrochemical sensor

1. Introduction

The development of enzymatic electrodes based on carbon materials with electrically-wired oxidoreductases is of great importance for biosensor and biofuel cell applications (Bollella and Katz, 2020; Gross et al., 2018). Carbon-based enzymatic electrodes have already shown remarkable commercial success for portable and wearable self-monitoring glucose sensors, and have tremendous potential for body-integrated and portable biofuel cells for low power electronics (Abreu et al., 2018a; Bollella et al., 2020; Chen et al., 2019; Lee et al., 2021). To date the glucose/O₂ biofuel cell is the most commonly reported and arguably most practical biofuel cell type; nevertheless, there are still important limitations relating to the stability and activity of the bioelectrodes as well as limited substrate availability. The oxygen reduction reaction at the cathode is typically achieved using the multicopper oxidases (MCOs) laccase or bilirubin oxidase (BOx), but such enzymes are degraded or inhibited by ubiquitous hydrogen peroxide and halogens such as chloride (Antiochia et al., 2019; Valles et al., 2020). Oxygen-dependent oxidases such as glucose oxidase (GOx) unfortunately generate hydrogen peroxide in the presence of oxygen. Chloride on the other hand is common in biological or artificial biofuel cell electrolytes. Laccases generally demonstrate good activity at acidic pH but low activity and/or stability at neutral pH (Goff et al., 2015). BOx is generally better-suited to neutral pH but BOx-based cathodes typically exhibit a *ca.* 100-200 mV lower onset potential ($E_{1/2(T1)} = 0.52 \text{ V vs. Ag/AgCl (sat. KCl) at pH 7.0}$) compared to laccases (Gross et al., 2017). Another prominent issue for MCO-based cathodes is related to the low concentration of dissolved oxygen (oxidant) in biological fluids: *ca.* 45-70 $\mu\text{mol L}^{-1}$ in blood and cerebrospinal fluid and *ca.* 200 $\mu\text{mol L}^{-1}$ in aqueous quiescent solutions (Gross et al., 2017; Zebda et al., 2018). The development of improved bioelectrode interfaces to address stability and substrate limitations whilst maintaining good mass and electron transport for effective catalytic activity is therefore highly desirable, not just for biofuel cells, but also for electrochemical biosensors.

Horseradish peroxidase (HRP) is a robust and readily available heme-containing glycoprotein capable of direct electron transfer (DET) bioelectrocatalytic $2 \text{ e}^-/2 \text{ H}^+$ reduction at carbon

electrodes such as graphite (Andreu et al., 2007; Ferapontova and Puganova, 2002), single-walled (Shu et al., 2016), double-walled (Agnès et al., 2013), and multi-walled carbon nanotubes (Abreu et al., 2018b; Elouarzaki et al., 2015) (MWCNTs), 3D printed graphene (López Marzo et al., 2020), and nanofiber composites (Jia et al., 2010). HRP is therefore an excellent candidate for the development of reagentless third generation H₂O₂ electrochemical biosensors (Xu et al., 2015). HRP bioelectrodes are also of interest to simplify biocathodes for biofuel cell applications, offering mediator-free bioelectrocatalysis at a high onset potential. The DET H₂O₂ reduction reaction with immobilised HRP has generally been obtained at potentials of *ca.* +100 to -50 mV *vs.* Ag/AgCl, although higher onset potentials up to *ca.* +400-600 mV *vs.* Ag/AgCl have been reported at oxygenated porous carbon and carbon nanotube electrodes (Jia et al., 2010; Ruff et al., 2017). Schuhmann, Stoica and coworkers made important developments on carbon fiber/CNT composites, highlighting the important roles of the hierarchically porous structure and the chemical functionalities, pyrene hexanoic or butyric acid, to achieve H₂O₂ reduction as high as +600 mV *vs.* Ag/AgCl (Jia et al., 2010; Ruff et al., 2018). Several studies highlighted the benefit of introducing oxygenated functionalities to the carbon surface, including specifically carboxylic acid groups, to improve hydrophilicity for DET bioelectrocatalysis (López Marzo et al., 2020; Yamamoto et al., 2003). Alternatively, we and others have demonstrated the possibility to obtain effective DET bioelectrocatalysis with HRP simply at nonfunctionalised MWCNTs that contain low levels of oxygen (*ca.* 1%)^[15,16].

As is also the case for MCO bioelectrodes, HRP bioelectrodes are limited by the low presence of endogenous substrate present in biological fluids for energy harvesting body-integrated biofuel cells, for example, operating in blood or sweat (Forman et al., 2016; Jia et al., 2012). An original approach in biofuel cell design to circumvent or minimise issues with low H₂O₂ concentration involves generating hydrogen peroxide *in-situ*, for example, via enzymatic reactions. Hydrogen peroxide may be continuously generated in situ from GOx (Abreu et al., 2018b; Elouarzaki et al., 2015; Jia et al., 2012; Gorton et al., 1991) or other oxidases such as pyranose oxidase (Lidén et al., 1998) or alcohol oxidase (AOx) (Ruff et al., 2017). Over 30 years ago, Kulys and Schmid demonstrated the concept of bienzyme electrodes based on peroxidase mixed with GOx, AOx or choline oxidase (Kulys and Schmid, 1990). ~~Over 20 years ago~~ Willner, Katz and coworkers demonstrated this ~~original~~ concept with GOx in solution at a microperoxidase-11 cathode compartment where GOx reduced O₂ to H₂O₂ (Willner et al., 1998). Lo gorton and coworkers provided a review showcasing the use of a

whole series of H₂O₂ producing oxidases with HRP at electrodes (Ruzgas et al., 1996). More recent developments focused on bi-enzymatic biocathodes with immobilised GOx/HRP (Agnès et al., 2013; Elouarzaki et al., 2015; Jia et al., 2012) and AOx/HRP (Ruff et al., 2017) where H₂O₂ was immediately generated in the vicinity of the cathode. At physiologically-relevant glucose concentrations in phosphate buffer saline (PBS, pH 7.4), without externally added peroxide, a practical current density of over 1 mA cm⁻² and a respectable 15 days storage stability was achieved for a co-immobilised GOx/HRP biocathode (Elouarzaki et al., 2015). More recently, we reported a flow-through portable biofuel cell in which unwired GOx at the anode generated H₂O₂ *in-situ* at the anode that was then transported to a HRP-based cathode, again, without the need to add peroxide from an external source. A respectable open circuit voltage (OCV) of 0.6 V and maximum power output of 0.7 mW for a single biofuel cell validated the potential of HRP-based cathodes as an alternative to O₂ biocathodes in glucose biofuel cells (Abreu et al., 2018b). Schuhmann and coworkers earlier validated the alternative AOx/HRP biocathode, relying on DET between MWCNTs and HRP, that was then integrated with a nicotinamide adenine dinucleotide (NAD)⁺-dependent alcohol dehydrogenase bioanode for a self-powered biofuel cell-biosensor (Ruff et al., 2017). A high OCV of 0.66 V and relatively low maximum power density of 8.9 μW cm⁻² were observed in air-saturated 0.5 M ethanol buffer solution. Another advantage for HRP biocathodes is their demonstrated high resistance to physiological concentrations of chloride at neutral pH (Jia et al., 2012; Shu et al., 2016). A direct comparative study showed better stability for HRP compared to laccase in the presence of chloride (Elouarzaki et al., 2015).

In the present work, we explore the use of several functional pyrene derivatives adsorbed at multi-walled carbon nanotube electrodes to shed new light on the influence of contrasting organic surface functionalities on DET bioelectrocatalysis with immobilised HRP. Concentration effects on catalytic current as well as voltage output and stability performance are considered for biocathode and biosensor applications. The construction of a new type of HRP bioelectrode incorporating hydrated nanocellulose as an environmentally friendly and sustainable component was subsequently investigated and the resulting sensor and catalytic stability performance evaluated.

2. Experimental Section

2.1. Materials and chemicals

Sodium phosphate dibasic (Na_2HPO_4 , $\geq 99\%$), sodium dihydrogen phosphate (NaH_2PO_4 , $\geq 99\%$), hydrogen peroxide ($\geq 30\%$ w/w in H_2O), 1-methyl-2-pyrrolidone (NMP, $\geq 99\%$), pyrene (98%, py), 1-pyrenebutyric acid N-hydroxysuccinimide ester (pyNHS, 95 %), 1-pyrenemethylamine hydrochloride (py NH_2 , 95 %), 1-pyrenebutyric acid (pyBA, 97%), 1-pyreneacetic acid (pyAA, 97 %), and horseradish peroxidase from *Armoracia rusticana* (type II, 150-250 units/mg solid) were purchased from Sigma Aldrich and used as received without further purification. The enzyme was stored at $-20\text{ }^\circ\text{C}$ when not in use. Distilled water was purified to a minimum resistivity of $15\text{ M}\Omega\text{ cm}^{-1}$ using a Millipore Ultrapure system. Commercial grade thin multi-walled carbon nanotubes (MWCNTs, $\text{Ø} = 9.5\text{ nm}$, 90% purity, NC7000, batch 1166) were obtained from Nanocyl and used as received without purification. High purity oxygen and argon were obtained from Messer. N, N-Dimethylformamide (DMF, 99.8%) was obtained from Carlo Erba reagents (France). Acetonitrile (ACN) was obtained from VWR chemicals (France). The 1 % bacterial cellulose nanofibers gel was obtained from Nano Novin Polymer Co. (99%, average 40 nm diameter) and used as received.

2.2. Electrochemistry

Electrochemical measurements were performed at room temperature using a Biologic VMP3 Multi Potentiostat operated with EC-lab software. A three-electrode cell was used comprising a carbon nanotube film-modified glassy carbon (GC) working electrode ($\text{Ø} = 3\text{ mm}$), a silver-silver chloride reference electrode (Ag/AgCl with saturated KCl), and a Pt wire counter electrode. GC electrodes were polished using a Presi polishing cloth with $1\text{ }\mu\text{m}$ alumina or diamond slurry then sonicated for 5 min in distilled water prior to use. Electrochemical experiments were performed in 0.1 mol L^{-1} phosphate buffer (pH 7.0) in the absence of oxygen. Oxygen was removed by purging the solution with argon for 15 min. A gentle argon flow was maintained in the air space above the solution during experiments. Amperometric data was recorded at $E_p = 0\text{ V vs. Ag/AgCl (sat. KCl)}$. Bioelectrodes were stored in fresh buffer solution between stability experiments performed on different days at 4°C in the fridge. Current densities were estimated based on the geometric surface area of the working electrode (0.071 cm^2).

2.3. Preparation of film-modified multiwalled carbon nanotube electrodes

5 mg of MWCNTs were first added to 2 mL of NMP in a sealed glass vial and the resulting suspension sonicated for 60-120 min to achieve a homogeneous dispersion. 20 μL of the MWCNT dispersion (2.5 mg mL^{-1}) was subsequently drop-casted onto the GC electrode to obtain a densely and homogeneously coated MWCNT layer after drying, based on our previously reported method (Gross et al., 2020). The modified electrode was dried under vacuum for *ca.* 2 hours then rinsed with 0.1 mol L^{-1} phosphate buffer (pH 7.0) prior to use.

2.4. Preparation of pyrene-modified MWCNT electrodes

The modified MWCNT electrodes were obtained by immersion of the electrode in a sealed vial containing 100 μL of 5 mmol L^{-1} modifier solution containing the pyrene derivative in DMF. After 60 min, the electrode was gently removed from the modifier solution then rinsed with DMF followed by ACN to remove weakly adsorbed species. The modified electrodes were rinsed gently with 0.1 mol L^{-1} phosphate buffer (pH 7.0) prior to use.

2.5. Preparation of HRP-modified MWCNT bioelectrodes

Aliquots of enzyme solution were first prepared at 5 mg mL^{-1} in 0.1 mol L^{-1} phosphate buffer (pH 7.0) and stored at -20°C . Prior to use, the aliquot was carefully thawed to room temperature then immediately used for bioelectrode preparation. The pyrene-modified MWCNT electrode was immersed in a sealed vial containing 40 μL of the enzyme solution then left overnight at 4°C in the fridge. Prior to electrochemistry or further modification, the bioelectrode surface was rinsed gently with 0.1 mol L^{-1} phosphate buffer (pH 7.0) to remove weakly adsorbed species.

2.6. Preparation of nanocellulose-modified HRP MWCNT bioelectrodes

2.6.1. Layer-by-layer method

The HRP modified bioelectrodes were first prepared as described in Section 2.5. 10 μL of the as-received nanocellulose gel (1% nanocellulose) was then mixed with 30 μL of 0.1 mol L^{-1} phosphate buffer (pH 7.0) in a vial for 60 s by vortexing. 20 μL of the mixture was then drop-

casted onto the bioelectrode. The electrode was left to dry at room temperature for 1 h then gently rinsed with the buffer solution prior to use.

2.6.2. One-pot method

0.4 mg of HRP, 10 μL of nanocellulose gel (1% nanocellulose) and 30 μL of 0.1 mol L^{-1} phosphate buffer (pH 7.0) were mixed together in a vial for 60 s by vortexing. After pre-rinsing of the pyrene-modified MWCNT electrode (Section 2.4) with the buffer, either 5 μL or 20 μL of the mixed enzyme/nanocellulose solution was drop-casted on the surface of the electrode. The electrode was left to dry at room temperature for 1 h then gently rinsed with the buffer solution prior to use.

3. Results and discussion

3.1. Bioelectrocatalysis of HRP/pyrene-modified MWCNT bioelectrodes

The pyrene and functionalised pyrenes employed for non-covalent modification of the MWCNT electrodes, and the subsequent preparation of HRP bioelectrodes for H_2O_2 reduction, are schematically illustrated in Figure 1.

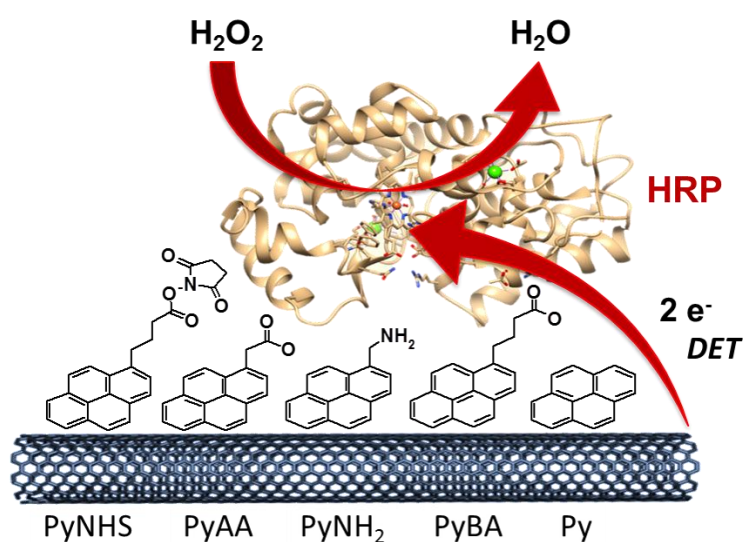


Figure 1. Schematic representation showing the five pyrene compounds used to obtain pyrene-modified MWCNT bioelectrodes with adsorbed HRP for the two-electron bioelectrocatalytic reduction of H_2O_2 to water. Enzyme structure pdb1H55 of HRP from *Armoracia rusticana* (Berglund et al., 2002).

The MWCNT electrodes were obtained according to our reported strategy that allows the formation of highly stable and reproducible MWCNT coatings on GC electrodes with a film thickness of *ca.* 6 μm (Gross et al., 2020; Lalaoui et al., 2016). The pyrene-modified MWCNT electrodes were prepared by a simple immersion protocol using a DMF modifier solution with 5 mmol L^{-1} of the pyrene derivative, followed by rinsing to remove weakly adsorbed species (Section 2.4). The effective adsorption of pyrenes including mono/polycyclic and ionisable/non-ionisable derivatives to CNTs occurs via physical interactions, particularly pi-pi stacking interactions between CNT sidewalls and the aromatic system of the molecules (Chunping et al., 2014; Haddad et al., 2010; Sheng et al., 2010). This non-covalent modification strategy is attractive for electrochemical biosensor and biofuel cell applications due to its simplicity, the ability to preserve the aromatic systems and therefore electronic properties of the nanotubes, and the possibility to introduce a wide range of surface functionalities in a straightforward manner (Gross et al., 2017; Haddad et al., 2010; Gutiérrez-Sánchez et al., 2012). For example, carbon nanotube electrodes modified with pyrene derivatives have been used to yield direct electron transfer with oxidoreductase enzymes such as laccase (Gutiérrez-Sánchez et al., 2012) and bilirubin oxidase (Mazurenko et al., 2016).

To achieve efficient DET bioelectrocatalysis with metalloenzymes it is necessary to optimise enzyme orientation and immobilisation. Recent studies have highlighted the importance of electrode functionalisation with ionisable, hydrophilic/hydrophobic, reactive tether, and/or substrate-like functional groups (Blanford et al., 2007; Lalaoui et al., 2016; Ramasamy et al., 2010; Tominaga et al., 2008). Concerning DET bioelectrocatalysis with HRP, several reports have shown the importance of surface oxygen functionalities and/or carboxylic acid groups to improve performance compared to unmodified carbon and CNT electrodes (Abreu et al., 2018b; Jia et al., 2010; López Marzo et al., 2020; Ruff et al., 2018; Shu et al., 2016; Yamamoto et al., 2003). Little progress has been made regarding the influence of charge and/or other surface functionalities to promote DET bioelectrocatalysis with immobilised HRP. The commercial HRP has a stated isoelectric point (pI) of approximately 3 to 9 owing to the presence of several isozymes. Nevertheless, important studies by Radola and Delincée on the fractionation of commercially-sourced HRP shows that the predominant isozyme pI is 9.1 (Delincée and Radola, 1975; Delincée and Radola, 1978). At pH 7.0 we therefore expect HRP to be positively charged. As depicted in Scheme 1, we explored the use of a “classical” pyrene-aliphatic carboxylic acid, pyrene butyric acid (pyBA, pK_a 4.8), as well as the shorter chain equivalent, pyrene acetic acid (pyAA, pK_a 4.2), a pyrene aliphatic amine (pyNH₂, $\text{pK}_b \sim$

10), pyrene, and a pyrene-NHS ester derivative. With all aqueous experiments performed in 0.1 mol L⁻¹ phosphate buffer (pH 7.0), this set of derivatives enabled the comparison of positive (protonated amine), negative (deprotonated carboxylic acid) and neutral (pyrene) charged surface species. Furthermore, the pyNHS derivative comprises the succinimidyl group that may react with amino residues at the surface of the enzyme to form strong covalent bonds, therefore enabling comparison of a “tether” functionality (Karachevtsev et al., 2011). The use of pyrene-NHS has proven to be very effective for DET bioelectrocatalysis with multicopper oxidases for O₂ reduction (Gross et al., 2018; Ramasamy et al., 2010) and is therefore an interesting alternative to electrostatic enzyme immobilisation.

Catalytic cyclic voltammetry experiments were performed in argon-saturated 0.1 mol L⁻¹ phosphate buffer (pH 7.0) for the unmodified and pyrene-modified electrodes after immobilisation of HRP by an immersion protocol then gentle rinsing (Section 2.5). Figure 2 shows the first-scan cyclic voltammograms (CVs) recorded at the MWCNT bioelectrodes from open circuit potential to 0 V vs. Ag/AgCl (sat. KCl) in the presence of “low” 0.5 mmol L⁻¹ and “high” 4 mmol L⁻¹ H₂O₂. CVs recorded in the absence of H₂O₂ showed no reduction processes beyond the background signal of the MWCNT bioelectrode (data not shown). In the presence of 0.5 mmol L⁻¹ H₂O₂, a large catalytic reduction peak is observed at all electrodes, including the unmodified electrode, consistent with DET bioelectrocatalysis between adsorbed HRP and the MWCNT electrodes (Figure 2A). Based on previous findings, the reaction occurs via the oxyferryl iron-porphyrin pi-cation radical species, Fe^{IV}=O,P⁺, of the active site of HRP Compound 1 (Jia et al., 2010). Similar catalytic current maximums of -21 to -24 μA are observed for the different pyrene-modified electrodes compared to a slightly lower current of -20 μA for the unmodified MWCNTs electrode, consistent with surface modification leading to a minor enhancement in DET at 0.5 mmol L⁻¹ H₂O₂. The pyBA bioelectrode exhibited the highest catalytic current but with unattractively low peak and onset potentials of 0.1 V and 0.49 V, respectively. PyNHS- and pyAA-modified bioelectrodes provided access to the highest onset potentials of 0.61 V and 0.60 V, respectively. The onset potentials are very close to the formal potential of 0.63 V for the redox conversion of HRP compound 1/ferric HRP at pH 7.0 vs. Ag/AgCl (Csöregi et al., 1993). The catalytic improvements observed with pyNHS, pyBA and pyAA indicate that hydrophilic and negatively-charged functionalities, or tether group functionalities, are more favorable compared to positively-charged or entirely hydrophobic modifications at “low” H₂O₂ concentration. Nevertheless, the hydrophobic bioelectrode prepared with pyrene still

exhibited enhanced bioelectrocatalysis compared to the unmodified MWCNT electrode. The negatively-charged functionalities that provide catalytic improvements compared to positively-charged functionalities highlight the beneficial electrostatic interactions at pH 7 that favor DET bioelectrocatalysis between positively-charged HRP enzymes and deprotonated aliphatic acids at the electrode. Figure 2 also shows the variable presence of an apparent redox couple at 0.1 V. Control experiments in Figure 2C and Figure S1 performed at CNT electrodes in the absence and presence of adsorbed HRP, respectively, indicate that these redox peaks originate from the carbon nanotubes. The redox peaks are tentatively attributed to surface quinone functionalities with a nature similar to those observed at MWCNT and graphite electrodes (Gusmão et al., 2015; Csöregi, 1993; Blanchard 2019).

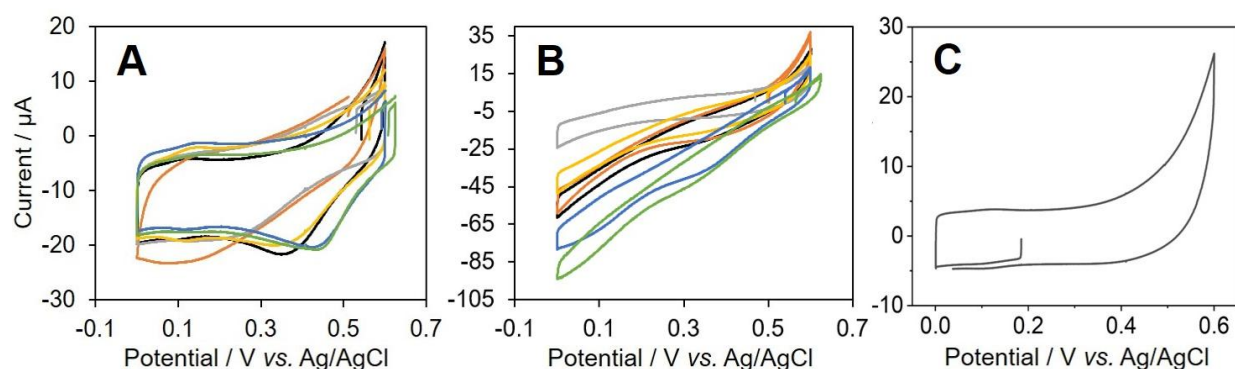


Figure 2: (A, B) CVs recorded at MWCNT-HRP bioelectrodes at 10 mV s⁻¹ in 0.1 mol L⁻¹ phosphate buffer (pH 7.0) with (A) 0.5 mmol L⁻¹ and (B) 4 mmol L⁻¹ H₂O₂: (□) unmodified; (□) py; (□) pyNHS; (□) pyAA; (□) pyBA; (□) pyNH₂. (C) CV recorded from open-circuit potential at unmodified MWCNT without HRP at 10 mV s⁻¹ in 0.1 mol L⁻¹ phosphate buffer (pH 7.0) with 4 mmol L⁻¹ H₂O₂.

At 4 mmol L⁻¹ H₂O₂, markedly different bioelectrocatalytic voltammograms with a more complex wave shape were observed (Figure 2B). The H₂O₂ concentration became sufficiently high that notable differences in maximum catalytic currents were observed between the modified electrodes. Generally, with an increase in substrate, higher catalytic currents were observed, particularly at lower potentials of *ca.* 0 to 0.1 V. The catalytic wave onset potential observed for pyNHS and pyAA again starts at *ca.* 0.6 V *vs.* Ag/AgCl, as observed at the “low” H₂O₂ concentration, which favorably compares to the 0.55 V *vs.* Ag/AgCl (pH 7.5) (Ruff et al., 2016) and 0.6 V maximum (pH 7) *vs.* Ag/AgCl (Jia et al., 2010) observed at previous high performing MWCNT DET HRP biocathodes. Such biocathodes clearly offer improved voltage performance compared to cross-linked CNT/HRP on thiol-modified gold (Kafi et al., 2018) with onset potentials starting at -0.05 V *vs.* Ag/AgCl at pH 7. The second reduction wave is characteristic of a catalytic “boost” linked to an increase in enzymatic

activity with driving force. A similar wave shape with a “boost” at low potential was reported by Armstrong and coworkers for fumarate reductase at a graphite electrode in the presence of high substrate concentration (Hudson et al., 2005). It may be that the DET mechanism takes a different route depending on the potential but this was not studied further. The possibility of an MET or mixed DET/MET mechanism at low potential involving the proposed surface quinone at bare CNTs is not ruled out (Csöregi, 1993). A control experiment performed at a MWCNT electrode without HRP in the presence of $4 \text{ mmol L}^{-1} \text{ H}_2\text{O}_2$ did not show any reductive currents, confirming that the second reduction wave observed in Figure 2B is not due to H_2O_2 reduction at unmodified MWCNTs (Figure 2C). PyNHS and pyAA bioelectrodes exhibited the highest catalytic currents of $-94 \text{ }\mu\text{A}$ and $-78 \text{ }\mu\text{A}$ compared to $-24 \text{ }\mu\text{A}$ observed at the unmodified MWCNT bioelectrode. This represents a 3-4 factor catalytic enhancement and the possibility to achieve up to *ca.* 1.1 to 1.3 mA cm^{-2} current densities for the tether function and shorter chain acid function. PyBA bioelectrodes produced a mediocre current maximum of $-50 \text{ }\mu\text{A}$ and globally weaker bioelectrocatalysis compared to the pyNHS and pyAA bioelectrode. The pyrene and pyNH₂ behaved similarly to the pyBA bioelectrodes, thus at “high” 4 mmol L^{-1} concentration, the positive, negative and neutral charges do not play a key role on enhanced DET bioelectrocatalysis. There is no obvious trend due to the use of different aliphatic chain lengths. For reference, voltammograms were not investigated at lower potentials of $\geq -0.15 \text{ V}$ where deactivation of the HRP is observed (Csöregi et al., 1993).

In addition to the bioelectrocatalytic H_2O_2 reduction behaviour, an oxidative response was also observed at the pyrene-modified MWCNT electrodes, as shown in Figure 2. The oxidative response corresponds to direct electrochemical oxidation of H_2O_2 , as previously reported at carbon electrodes (Jia et al., 2010). The H_2O_2 oxidation occurring at $\geq 0.52 \text{ V}$ therefore competes with the reduction process and diminishes the H_2O_2 reduction current at these bioelectrodes. Considering both 0.5 mmol L^{-1} and 4 mmol L^{-1} concentrations, the most effective bioelectrodes for the parasitic H_2O_2 oxidation are pyBA and pyNH₂ while the least effective was the pyNHS bioelectrode. The insensitivity of the pyrene-NHS bioelectrode towards H_2O_2 is consequently one of the important factors that permits high catalytic H_2O_2 reduction performance, particularly at the “high” peroxide concentration.

The steady-state amperometric current responses of the unmodified and pyrene-modified HRP bioelectrodes were subsequently measured at 0 V vs. Ag/AgCl under hydrodynamic

conditions from 0.25 mmol L⁻¹ to 9 mmol L⁻¹. Figure 3 shows the current-concentration response curves obtained from the amperometric experiments. The unmodified and modified electrodes show the same general trend with a linear increase in current to a plateau followed by a drop-off in current. Linear calibration curves ($r^2 \geq 0.98$) from 0.25 mmol L⁻¹ to between 1 mmol L⁻¹ and 4 mmol L⁻¹ were observed, depending on the pyrene derivative used (Figure S2). The pyNHS and pyAA bioelectrodes delivered the highest catalytic currents of 98.5 μA (1.4 mA cm⁻²) and 86.5 μA (1.2 mA cm⁻²) at 6 mmol L⁻¹, respectively. Beyond 6 mmol L⁻¹ the catalytic current decreases as a result of enzyme deactivation. Such HRP “suicide inactivation” has previously been observed at low millimolar concentrations of H₂O₂, occurring when the peroxide converts Compound 2 of HRP into a highly reactive peroxy iron(III) porphyrin free radical that subsequently decomposes (Malomo et al., 2011). For a biocathode or biosensor targeting the highest catalytic current or wider dynamic range, the pyNHS is the optimal electrode. If higher catalytic currents or better sensor sensitivity is required at ≤ 1 mmol L⁻¹ concentrations, then the pyBA or pyAA bioelectrode is the better choice. The sensitivities for pyBA and pyNHS bioelectrodes are 5.63 A M⁻¹ cm⁻² (0.40 A M⁻¹) and 2.96 A M⁻¹ cm⁻² (0.21 A M⁻¹) (Figure S2). These analytical sensitivities are high performance compared to estimated values of 0.15 A M⁻¹ at activated graphene (López Marzo et al., 2020), 0.298 A M⁻¹ cm⁻² at cross-linked Os redox polymer and modified graphite (Bollella et al., 2018), 0.12 A M⁻¹ cm⁻² at carbon microspheres with integrated chitosan (Chen et al., 2008), or *ca.* 0.0026 A M⁻¹ at a polymer-based CNT electrode (Moyo et al., 2013), or 0.34 A M⁻¹ at a cross-linked CNT on thiol-modified Au electrode (Kafi et al., 2018). The pyBA bioelectrode notably also offers improved analytical sensitivity compared to the high sensitivity of 4.25 A M⁻¹ cm⁻² achieved at an ultramicroelectrode DET biosensor integrating ionic liquid, carbon fibers and single-walled CNTs (Ren et al., 2017), or a DET biosensor based on commercial screen-printed carbon electrodes with single-walled CNTs (Chekin et al., 2015) that yielded 0.0051 A M⁻¹ cm⁻².

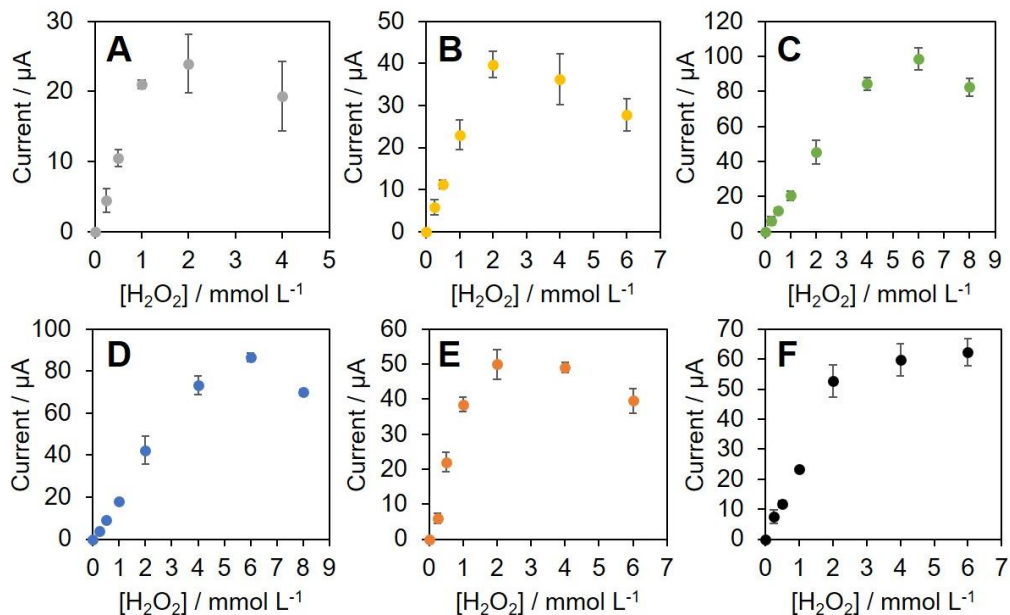


Figure 3: Amperometric current-concentration response curves recorded at MWCNT-HRP electrodes in 0.1 mol L⁻¹ phosphate buffer (pH 7.0) before and after additions of H₂O₂ at increasing concentrations: (A, •) unmodified; (B, •) py; (C, •) pyNHS; (D, •) pyAA; (E, •) pyBA; (F, •) pyNH₂. Current values obtained at 0 V vs. Ag/AgCl. Error bars correspond to standard deviation from $n = 3$ samples.

3.2. Bioelectrocatalysis of pyrene-NHS modified HRP bioelectrodes with nanocellulose

Towards the development of eco-friendlier biosensor and biofuel cell devices with improvements in properties such as biocompatibility and stability, we explored the development of HRP bioelectrodes integrating bacterial nanocellulose. Bacterial nanocellulose is a natural cellulosic fibrous material that offers advantages such as excellent biocompatibility, biodegradability, hydrophilicity and hydrogel-forming properties at very low solid content via -OH groups, high specific surface area and porous nanofibrillar network, eco-friendly processing, and low production costs (Abol-Fotouh et al., 2020; Stanisławska, 2016). Tominaga and coworkers reported the construction of a “one-pot” nanocellulose/CNT laccase biocathode, citing the possibility to improve electrode flexibility and proton conductivity; however, performance was limited compared to other biocathodes and no stability or biocompatibility data was reported (Tominaga et al., 2020). Slaughter and coworkers integrated bacterial nanocellulose sheets with bioelectrodes as a flexible and biocompatible layer to contact with skin (Yuen et al., 2019). The nanocellulose was however *not* exploited as part of the catalytic matrix to enhance bioelectrocatalysis. Zhang and coworkers developed a second-generation HRP biosensor based on gold nanoparticles with a

quinone mediator and bacterial cellulose that offered high performance with a sensitivity of $0.61 \text{ A M}^{-1} \text{ cm}^{-2}$ (Wang et al., 2011). The absence of comparative data limits makes it difficult to define the enhancement effects specifically related to the nanocellulose.

We developed a nanocellulose bioelectrode design that is illustrated in Figure 4A. The pyrene-NHS modified MWCNT electrode was chosen due to the promising results observed for both biocathode and biosensor applications. Two strategies were investigated: (i) “layer-by-layer” with nanocellulose added as an outer layer to the pyNHS HRP bioelectrode, and (ii) a “one-pot” strategy with a mixture of nanocellulose and enzyme first prepared then added as a mixed layer to the pyNHS electrode (see Section 2.6). Figure 4B shows the CVs obtained at the optimised nanocellulose/pyNHS bioelectrode prepared by the one-pot ($5 \mu\text{L}$) method. The CVs were obtained from 0.6 V to 0 V before after the addition of increasing amounts of H_2O_2 from 0.4 mmol L^{-1} to 8 mmol L^{-1} . At concentrations $\leq 2 \text{ mmol L}^{-1}$, well-defined catalytic reduction peaks are observed that are followed by a slightly lower but constant current, consistent with the current not being diffusion limited, despite the presence of cellulosic material in the catalytic layer.

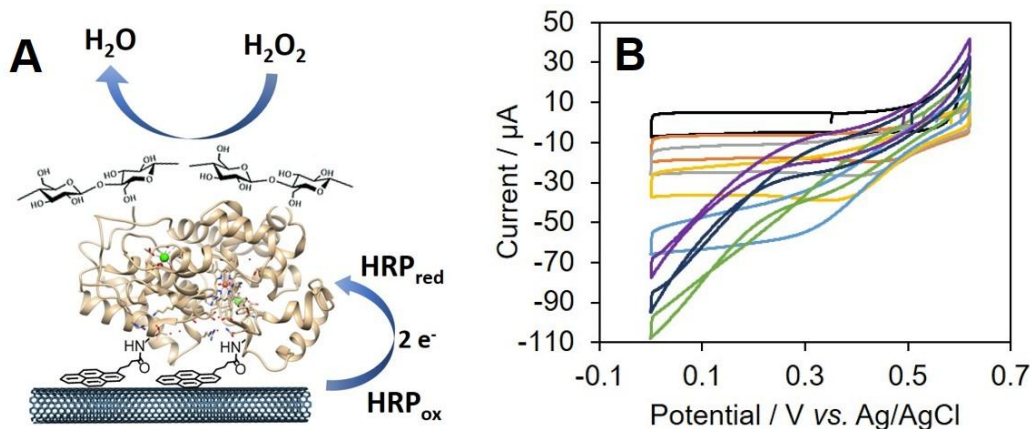


Figure 4: Schematic representation of the MWCNT-HRP electrodes modified with pyNHS and nanocellulose. (B) Representative CVs recorded at 10 mV s^{-1} at the one-pot ($5 \mu\text{L}$) nanocellulose/pyNHS HRP bioelectrode in 0.1 mol L^{-1} phosphate buffer (pH 7.0) before and after addition of H_2O_2 at (\square) 0.4 ; (\square) 0.6 ; (\square) 1 ; (\square) 2 ; (\square) 4 ; (\square) 6 ; and (\square) 8 mmol L^{-1} .

The CVs recorded at “low” and “high” millimolar H_2O_2 concentrations for the one-pot ($5 \mu\text{L}$) nanocellulose/pyNHS HRP bioelectrode (Figure 4B) are similar to those observed at the pyNHS HRP bioelectrode without nanocellulose (Figure 2A), except for a few differences at $4 \text{ mmol L}^{-1} \text{ H}_2\text{O}_2$. First, a higher catalytic current of $110 \mu\text{A}$ (1.6 mA cm^{-2}) and the highest in this study was observed at the one-pot ($5 \mu\text{L}$) nanocellulose/pyNHS HRP bioelectrode,

representing a 17% increase compared to the pyNHS HRP bioelectrode output at the same H_2O_2 concentration. The other difference is that CVs observed at one-pot (5 μL) nanocellulose/pyNHS HRP bioelectrode at 4 mmol L^{-1} (and 6 mmol L^{-1}) exhibited two unusual voltage cross-over points at low potential, but their nature is unclear. The crossed CVs may be related to changes in nucleation and/or conductivity of the cellulosic fibers, or result from enzyme activation and deactivation processes that switch abruptly at certain potentials.

Figure 5 shows the current-concentration response curves for the unmodified and pyrene-NHS modified HRP bioelectrode vs. the one-pot (5 μL) nanocellulose/pyNHS HRP bioelectrodes. Figure 5A and Figure 5B reveal either similar or enhanced catalytic current output as well as better sensitivity performance ($3.51 \text{ A M}^{-1} \text{ cm}^{-2}$) across the current range from 0.25 mmol L^{-1} to 8 mmol L^{-1} for the optimised nanocellulose bioelectrode compared to the pyNHS and unmodified bioelectrodes without nanocellulose.

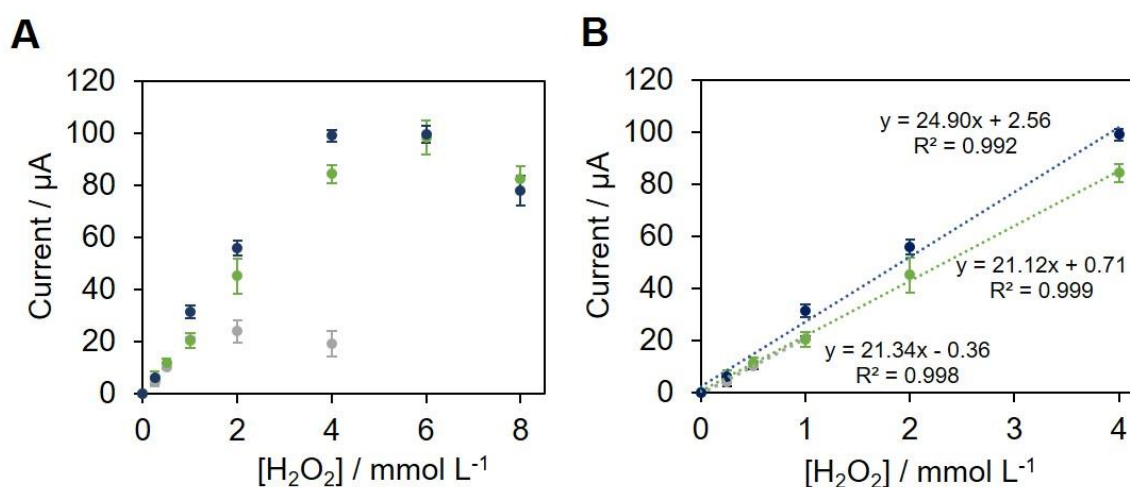


Figure 5. Current-concentration (A) full range and (B) linear dynamic range response curves recorded at MWCNT-HRP electrodes in 0.1 mol L^{-1} phosphate buffer (pH 7.0) before and after increasing additions of H_2O_2 : (•) unmodified; (•) pyNHS; (•) one pot (5 μL) nanocellulose/pyNHS. Current values obtained at 0 V vs. Ag/AgCl. Error bars correspond to standard deviation from $n = 3$ samples.

Current-concentration responses for the alternative one-pot (20 μL) and layer-by-layer nanocellulose/pyNHS HRP bioelectrodes are reported in Figure S3. Significantly smaller catalytic currents were observed for these alternative configurations. The most important difference between the alternative nanocellulose preparations and the optimised preparation is that 300% more enzyme and nanocellulose were used for the alternative nanocellulose

electrodes. Therefore, it seems likely that the nanocellulose at the alternative electrodes, possibly involving a synergetic effect with enzyme, hinders effective orientation and electron transport between the HRP and the pyNHS-modified CNTs. The alternative one-pot (20 μL) bioelectrode gave approximately two-fold higher catalytic currents compared to the alternative “layer-by-layer (20 μL)” bioelectrode prepared using the same amounts of enzyme and nanocellulose (Figure S3). The incorporation of nanocellulose *in* the enzyme layer (one-pot) as opposed to *on* the enzyme layer (layer-by-layer) therefore has a drastic positive effect on the catalytic current. The superior catalytic currents at layer-by-layer compared to one-pot can be explained by two important effects. The first, that the one-pot electrode has increased hydrophilicity and therefore hydration across the bulk nanocellulose-CNT matrix that increases the amount of electrochemically-wired HRP in the porous electrode structure. And second, a steric and/or electrically insulating barrier effect for the layer-by-layer electrode that limits H_2O_2 permeation and enzyme wiring, respectively.

Next our attention focused on evaluating the open-circuit potential (OCP) as an indicator of effective bioelectrocatalysis and as a useful parameter of a biocathode for estimating the maximum possible operating voltage of a biofuel cell. The OCP is the potential adopted by the electrode at zero current and in this case reflects the highest potential at which the enzyme is capable of DET with the electrode, being typically close to the onset potential for bioelectrocatalytic reduction (Mano and de Poulpiquet, 2017). Figure 6A shows the loss in OCP at an increasingly slower rate with increasing additions of H_2O_2 for the one pot (5 μL) nanocellulose bioelectrode. A high and stable OCP and onset potential is highly desirable, particularly for biocathodes with the objective of boosting the voltage output of biofuel cells. Despite the slightly weaker OCP performance by *ca.* 5% for the nanocellulose bioelectrode, the OCP values of between 0.5 to 0.62 V at $\leq 6 \text{ mmol L}^{-1} \text{ H}_2\text{O}_2$ remain in a very practical range for a biocathode.

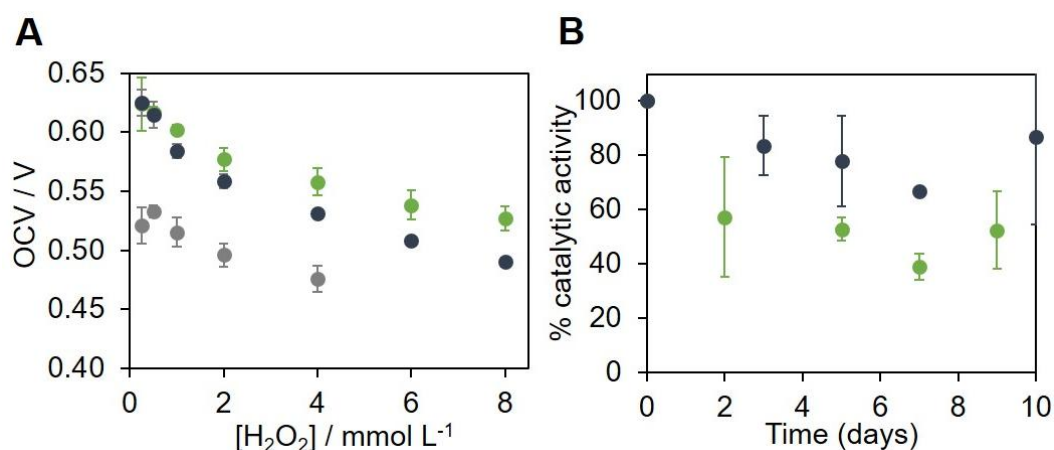


Figure 6: (A) Open circuit voltage-concentration plot recorded at MWCNT-HRP electrodes in 0.1 M phosphate buffer (pH 7.0) before and after increasing additions of H_2O_2 : (•) unmodified; (•) pyNHS; (•) pyNHS-nanocellulose. (B) Bioelectrocatalytic current from CVs recorded at (•) pyNHS and (•) pyNHS-nanocellulose modified MWCNT-HRP electrodes in 0.1 mol L^{-1} phosphate buffer (pH 7.0) in 4 $mmol L^{-1}$ H_2O_2 : (•) unmodified; (•) pyNHS; (•) nanocellulose/pyNHS. Current values obtained at 0 V vs. Ag/AgCl.

Bioelectrocatalytic stability experiments were performed over a 9-10 day period at the modified electrodes. Figure 6B shows a plot of the catalytic currents measured in the presence of 4 $mmol L^{-1}$ H_2O_2 at 0 V vs. Ag/AgCl from cyclic voltammograms recorded at 10 $mV s^{-1}$ from 0.6 V to 0 V. The bioelectrodes were stored in 0.1 M phosphate buffer (pH 7) solution free of H_2O_2 in the fridge at 4°C. The stability profiles for the pyNHS and nanocellulose/pyNHS bioelectrodes show the same general trend. However, of particular interest, the nanocellulose bioelectrodes exhibit a dramatic enhancement in stability with an average of 67% of the initial activity remaining after 7 days compared to 39% after 7 days for the pyNHS modified bioelectrode without nanocellulose.

Conclusion

The non-covalent modification of multi-walled carbon nanotube electrodes with various pyrene derivatives is a simple and versatile method to promote DET bioelectrocatalysis with immobilised HRP for H_2O_2 . Surface modification with NHS ester and butyric acid groups proved the most effective for both high and low “catalytic boost” potential bioelectrocatalytic H_2O_2 reduction, and most resistant to parasitic H_2O_2 electro-oxidation. Integration of bacterial nanocellulose by a straightforward one-pot protocol is an extremely promising method that not only enhanced catalytic current output while maintaining a very respectable open circuit potential performance, but also significantly improved the catalytic stability, offering 72%

more stability, compared to the equivalent electrode without the nanocellulose. The nanocellulose strategy in principle can be used with any other enzyme at functionalised MWCNT electrodes to improve the activity and stability of a wide range of catalytic bioelectrodes for biosensor and biofuel applications. The nanocellulose biocathode, and future nanocellulose bioelectrodes, may also provide attractive biocompatibility, biodegradability, and mechanical properties for body-integrated applications but this remains to be explored. Future work integrating HRP and HRP bi-enzymatic electrodes for biofuel cell applications is envisioned.

Acknowledgments

The authors would like to thank the Generalitat Valenciana (PROMETEO Program 2016/109 and 2020/078) for financial support. SB expresses her gratitude to the PROMETEO program for her pre-doctoral grant and the GV-Union Social Fund for the foreign research visit grant (BEFPI19). The authors gratefully acknowledge support from the platform Chimie NanoBio ICMG FR 2607 (PCN-ICMG), and financial support from the French Agence Nationale de la Recherche (ANR) under reference ANR-20-CE05-0006-01 (JCJC), and LabEx ARCANÉ (ANR-11-LABX-003-01) and CBH-EUR-GS (ANR-17-EURE-0003).

Declaration of Competing Interest

The authors declare that they have no known competing financial interests or personal relationships that could have appeared to influence the work reported in this paper.

References

- Abol-Fotouh, D., Hassan, M.A., Shokry, H., Roig, A., Azab, M.S., Kashyout, A.E.-H.B., 2020. *Sci. Rep.* 10, 3491.
- Abreu, C., Nedellec, Y., Ondel, O., Buret, F., Cosnier, S., Le Goff, A., Holzinger, M., 2018a. *Sens. Actuators B Chem.* 277, 360.
- Abreu, C., Nedellec, Y., Ondel, O., Buret, F., Cosnier, S., Le Goff, A., Holzinger, M., 2018b. *J. Power Sources* 392, 176.
- Agnès, C., Reuillard, B., Le Goff, A., Holzinger, M., Cosnier, S., 2013. *Electrochem. Commun.* 34, 105.
- Andreu, R., Ferapontova, E.E., Gorton, L., Calvente, J.J., 2007. *J. Phys. Chem. B* 111, 469.
- Antiochia, R., Oyarzun, D., Sánchez, J., Tasca, F., 2019. *Catalysts* 9, 1056.
- Berglund, G.I., Carlsson, G.H., Smith, A.T., Szöke, H., Henriksen, A., Hajdu, J., 2002. *Nature* 417, 463.

Blanchard, P.-Y., Buzzetti, P.H.M., Davies, B., Nedellec, Y., Giroto, E. M. Gross, A. J., Le Goff, A., Nishina, Y., Cosnier, S., Holzinger, M., 2019. *ChemElectroChem* 6, 5242.

Blanford, C.F., Heath, R.S., Armstrong, F.A., 2007. *Chem. Commun.* 0, 1710.

Bollella, P., Katz, E., 2020. *Sensors* 20, 3517.

Bollella, P., Lee, I., Blaauw, D., Katz, E., 2020. *ChemPhysChem* 21, 120.

Bollella, P., Medici, L., Tessema, M., Poloznikov, A.A., Hushpulia, D.M., Tishkov, V.I., Andreu, R., Leech, D., Megersa, N., Marcaccio, M., Gorton, L., Antiochia, R., 2018. *Solid State Ion.* 314, 178.

Chen, X., Li, C., Liu, Y., Du, Z., Xu, S., Li, L., Zhang, M., Wang, T., 2008. *Talanta* 77, 37.

Chen, X., Yin, L., Lv, J., Gross, A.J., Le, M., Gutierrez, N.G., Li, Y., Jeerapan, I., Giroud, F., Berezovska, A., O'Reilly, R.K., Xu, S., Cosnier, S., Wang, J., 2019. *Adv. Funct. Mater.* 29, 1905785.

Chekin, F., Gorton, L., Tapsobea, I., 2015. *Anal. Bioanal. Chem* 407, 439.

Chunping H., Shimada M., Okamoto Y., Hijikata H., Watanabe K., 2014. *Surf. Sci.* 35, 340.

Csöregi, E., Jönsson-Pettersson, G., Gorton, L., 1993. *J. Biotechnol.* 30, 315.

Delincée, H., Radola, B.J., 1975. *Eur. J. Biochem.* 52, 321.

Delincée, H., Radola, B.J., 1978. *Anal. Biochem.* 90, 609.

Elouarzaki, K., Bourourou, M., Holzinger, M., Le Goff, A., Marks, R.S., Cosnier, S., 2015. *Energy Environ. Sci.* 8, 2069.

Ferapontova, E., Puganova, E., 2002. *J. Electroanal. Chem.* 518, 20.

Forman, H.J., Bernardo, A., Davies, K.J.A., 2016. *Arch. Biochem. Biophys.* 603, 48.

Goff, A.L., Holzinger, M., Cosnier, S., 2015. *Cell. Mol. Life Sci.* 72, 941.

Gorton, L., Bremle, G., Csöregi, E., Jönsson-Pettersson, G., Persson, B., 1991. *Anal. Chim. Acta*, 249, 43.

Gross, A.J., Chen, X., Giroud, F., Abreu, C., Le Goff, A., Holzinger, M., Cosnier, S., 2017. *ACS Catal.* 7, 4408.

Gross, A.J., Holzinger, M., Cosnier, S., 2018. *Energy Environ. Sci.* 11, 1670.

Gross, A.J., Tanaka, S., Colomies, C., Giroud, F., Nishina, Y., Cosnier, S., Tsujimura, S., Holzinger, M., 2020. *ChemElectroChem* 7, 4543.

Gusmão, R., Melle-Franco, M., Geraldo, D., Bento, F., Paiva, M., Proença F., 2015. *Electrochem. Commun.* 57, 22.

Gutiérrez-Sánchez, C., Jia, W., Beyl, Y., Pita, M., Schuhmann, W., De Lacey, A. L., Stoica, L., 2012. *Electrochim. Acta.* 82, 218.

Haddad, R., Holzinger, M., Maaref, A., Cosnier, S., 2010. *Electrochimica Acta.* 7800.

Hudson, J.M., Heffron, K., Kotlyar, V., Sher, Y., Maklashina, E., Cecchini, G., Armstrong, F.A., 2005. *J. Am. Chem. Soc.* 127, 6977.

Jia, W., Jin, C., Xia, W., Muhler, M., Schuhmann, W., Stoica, L., 2012. *Chem. – Eur. J.* 18, 2783.

Jia, W., Schwamborn, S., Jin, C., Xia, W., Muhler, M., Schuhmann, W., Stoica, L., 2010. *Phys. Chem. Chem. Phys.* 12, 10088.

Kafi, A.K.M., Naqshabandi, M., Yusoff, M.M., Crossley, M.J., 2018, *Enzyme Micro. Technol.* 113, 67.

Kulys, J., Schmid, R.D., 1990, *Bielectrochem. Bioenerg.* 24, 305.

Karachevtsev, V.A., Stepanian, S.G., Glamazda, A.Yu., Karachevtsev, M.V., Eremenko, V.V., Lytvyn, O.S., Adamowicz, L., 2011. *J. Phys. Chem. C* 115, 21072.

Lalaoui, N., Holzinger, M., Le Goff, A., Cosnier, S., 2016. *Chem. - Eur. J.* 22, 10494.

Lee, D., Jeong, S.H., Yun, S., Kim, S., Sung, J., Seo, J., Son, S., Kim, J.T., Susanti, L., Jeong, Y., Park, S., Seo, K., Kim, S.J., Chung, T.D., 2021. *Biosens. Bioelectron.* 171, 112746.

Lidén, H., Volc, J., Marko- Varga, G., Gorton, L., 1998. *Electroanalysis* 10, 223.

- López Marzo, A.M., Mayorga-Martinez, C.C., Pumera, M., 2020. *Biosens. Bioelectron.* 151, 111980.
- Malomo, S.O., Adeoye, R.I., Babatunde, L., Saheed, I.A., Iniaghe, M.O., Olorunniji, F.J., 2011. *Biokemistri* 23.
- Mano, N., de Poulpique, A., 2017. *Chem. Rev.* 118, 5, 2392.
- Mazurenko, I., Monsalve, K., Rouhana, J., Parent, P., Laffon, C., Le Goff, A., Szunerits., Boukherroub, R., Giudici-Ortoni, M-T., Mano, N., Lojou, E., 2016, *ACS. Appl. Mater. Interfaces.* 8. 23074.
- Moyo, M., Okonkwo, J.O., Agyei, N.M., 2013. *Electroanalysis* 25, 1946.
- Ramasamy, R.P., Luckarift, H.R., Ivnitski, D.M., Atanassov, P.B., Johnson, G.R., 2010. *Chem. Commun.* 46, 6045.
- Ren, Q-Q., Wu, J., Zhang, W-C., Wang, C., Qin, X., Liu G-C., Li, Z-X., Yu, Y., 2017, *Sens. Actuator B-Chem.* 245, 615.
- Ruff, A., Szczesny, J., Marković, N., Conzuelo, F., Zacarias, S., Pereira, I.A.C., Lubitz, W., Schuhmann, W., 2018. *Nat. Commun.* 9. 3675.
- Ruff, A., Pinyou, P., Nolten, M., Conzuelo, F., Schuhmann, W., 2017, *ChemElectroChem.* 4, 890.
- Ruzgas, T., Csöregi, E., Emnéus, J., Gorton, L., Marko-Varga, G., 1996. *Anal. Chim. Acta*, 330, 123.
- Sheng, G.D., Shao, D.D., Ren, X.M., Wang, X.Q., Li, J.X., Chen, Y.X., Wang, X.K., 2010. *J. Hazard. Mater.* 178, 505.
- Shu, T., Gao, B., Yang, H., Su, L., Zhang, X., 2016. *Curr. Nanosci.* 12, 405.
- Stanisławska, A., 2016. *Adv. Mater. Sci.* 16, 45.
- Tominaga, M., Kuwahara, K., Tsushida, M., Shida, K., 2020. *RSC Adv.* 10, 22120.
- Tominaga, M., Ohtani, M., Taniguchi, I., 2008. *Phys. Chem. Chem. Phys.* 10, 6928.
- Valles, M., F. Kamaruddin, A., Shin Wong, L., F. Blanford, C., 2020. *Catal. Sci. Technol.* 10, 5386.
- Wang, W., Zhang, T.-J., Zhang, D.-W., Li, H.-Y., Ma, Y.-R., Qi, L.-M., Zhou, Y.-L., Zhang, X.-X., 2011. *Talanta* 84, 71.
- Willner, I., Katz, E., Patolsky, F., Bückmann, A.F., 1998. *J. Chem. Soc. Perkin Trans. 2* 1817.
- Xu, S., Qin, X., Zhang, X., Zhang, C., 2015. *Microchim. Acta Online* 182, 1241.
- Yamamoto, K., Shi, G., Zhou, T., Xu, F., Xu, J., Kato, T., Jin, J.-Y., Jin, L., 2003. *Analyst* 128, 249.
- Yuen, J.D., Baingane, A., Hasan, Q., Shriver-Lake, L.C., Walper, S.A., Zabetakis, D., Breger, J.C., Stenger, D.A., Slaughter, G., 2019. *Sci. Rep.* 9.
- Zebda, A., Alcaraz, J.-P., Vadgama, P., Shleev, S., Minteer, S.D., Boucher, F., Cinquin, P., Martin, D.K., 2018. *Bioelectrochemistry* 124, 57.